Design and optimization of lattice structures for aerospace applications

Enrico Stragiotti

François-Xavier Irisarri[1], **Cédric Julien**[1] **and Joseph Morlier**[2]

1: ONERA - The French Aerospace Lab
DMAS - Département matériaux et structures
92320 Châtillon, France
{francois-xavier.irisarri, cedric.julien}@onera.fr

2: ICA - Institut Clément Ader
ISAE - SUPAERO
31400 Toulouse, France
joseph.morlier@isae-supaero.fr

September 9, 2023

PhD manuscript

ONERA – ISAE Supaero

Colophon
This document was typeset with the help of KOMA-Script and LaTeX using the kaobook class.

ONERA – ISAE Supaero

Contents

List of Figures

List of Tables

List of Abbreviations

DOFs Degrees Of Freedom
HS Hashin-Shtrikman
KS Kreisselmeier-Steinhauser
LP Linear Programming
MPVCs Mathematical Programs with Vanishing Constraints
NAND Nested Analysis and Design
SAND Simultaneous Analysis and Design
SIMP Solid Isotropic Material with Penalization Method
TTO Truss Topology Optimization

Evaluating discretization approaches for ultralight structure optimization 1

Part of the content presented in this chapter has been published and showcased during a conference as: Stragiotti, E. et al. (2021) "Towards manufactured lattice structures: a comparison between layout and topology optimization", in *AeroBest 2021 International Conference on Multidisciplinary Design Optimization of Aerospace Systems*. Book of proceedings. Lisbon, Portugal: ECCOMAS [1].

The process of topology optimization for a structure involves the selection and sizing of optimal elements within a predetermined set. As discussed in the previous chapter, in our context this set could be composed of either continuum elements (shell or volumetric) or truss-like elements. This chapter aims to assess the suitability and the inherent advantages and disadvantages of both methodologies when optimizing ultralight structures i.e. structures that exhibit an extremely low volume fraction, typically below 1%.

For this purpose, we initially establish a common optimization formulation in Section 1.1. The classic compliance minimization with volume constraint problem is reformulated as a volume minimization problem with maximum stress constraints for both discretization. Later, this framework is applied to optimize a two-dimensional test case, featuring identical dimensions, loads, and material properties. The outcomes of the comparison of both discretization approaches are presented and discussed in Section 1.2.

1.1 The formulation of a common problem: volume minimization with stress constraints

Two of the most frequently employed formulations for structural optimization are the minimization of volume while adhering to stress constraints and the minimization of compliance under volume constraints. Historically, the volume minimization formulation has been used in the first works of structural optimization of truss structures [2–4]. The problem was initially formulated in terms of member forces, ignoring the kinematic compatibility to obtain a Linear Programming (LP) problem. The formulation was modeled using the Simultaneous Analysis and Design (SAND) approach, where the equations of nodal equilibrium are treated as equality constraints, and where both nodal displacements and the cross-sectional areas of truss members serve as design variables [5].

However, to attain greater design freedom, the structure optimization field later transitioned from truss structures to continuous discretization. While truss structures offered simplicity and ease of analysis, they imposed limitations on design due to their discrete member configurations. The continuum mesh offered instead more versatility [6, 7], and has since been used for multiple different applications, e.g. the design of metamaterials [8, 9]. The SAND approach is incompatible with continuum meshes due to its excessive number of variables[1].

2. Dorn et al. (1964), 'Automatic design of optimal structures'
3. Chan (1964), 'Optimum structural design and linear programming'
4. Hemp (1973), *Optimum Structures*
5. Sankaranarayanan et al. (1994), 'Truss topology optimization with simultaneous analysis and design'
6. Bendsøe et al. (1988), 'Generating optimal topologies in structural design using a homogenization method'
7. Bendsøe (1989), 'Optimal shape design as a material distribution problem'
8. Sigmund (1994), 'Materials with prescribed constitutive parameters'
9. Zhang et al. (2006), 'Scale-related topology optimization of cellular materials and structures'

1: This preposition holds true when referring to the end of the 1980s, when computational power was scarce compared to what we have today.

Given this limitation, a new approach was required to better handle the complexity of continuum meshes.

In the Nested Analysis and Design (NAND) approach, the nodal displacement (state) variables are eliminated from the optimization problem through a process where the structural equilibrium equation is solved every iteration instead of being used as a constraint of the optimization. This results in an independent nested phase where the state equation of structural equilibrium is solved separately from the optimization algorithm. This creates a dense coupling between displacement and material density variables, necessitating a computationally expensive sensitivity analysis within the nested algorithm, typically employing the adjoint method (more information about the adjoint method on the following resurces [10, 11]). Nevertheless, if the problem is reformulated as a compliance minimization with volume constraints, the problem is self-adjoint and the adjoint algorithm is no longer necessary to evaluate the gradient sensitivities [12].

10. Tortorelli et al. (1994), 'Design sensitivity analysis'
11. Martins et al. (2021), *Engineering Design Optimization*
12. Bendsøe et al. (2004), *Topology Optimization*

However, our emphasis on operating within the aerospace sector aligns more favorably with the volume minimization problem. The choice to prioritize volume minimization in the aerospace sector is underpinned by a range of economic, environmental, and performance-related factors. It is a strategic approach that aligns with industry goals of sustainability, efficiency, and technological advancement. Additionally, as we will see later in this thesis, the volume minimization formulation will permit adding local buckling and maximum displacements constraints in an easier way. We have opted, thus, to employ the volume minimization optimization formulation for our study, and we will now review how this formulation is implemented on continuum and truss-like meshes.

1.1.1 Continuous discretization NAND minimum volume formulation

This section introduces the NAND volume minimization formulation of topology optimization for continuum meshes. We will start however presenting the more common minimum compliance formulation to explain the important notations and concepts that will be essential in developing the volume minimization formulation.

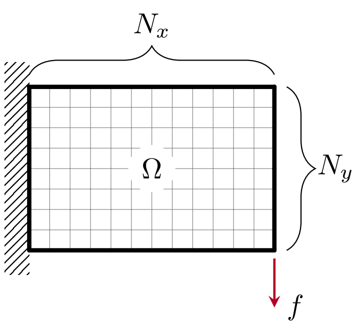

Figure 1.1: The domain Ω is discretized using $N_e = N_x N_y$ continuous 4-nodes elements.

Minimum compliance formulation Let $\Omega \in \mathbb{R}^2$ be a rectangular domain in of dimensions X and Y, containing respectively N_x and N_y linear 4-nodes elements, for a total of $N_e = N_x N_y$ elements and M nodes (see Fig. 1.1). The objective of the optimization is the minimization of the compliance C of the structure, equivalent to finding the structure with the least possible nodal displacement with respect to a defined set of boundary conditions. The problem $\mathbb{T}_0$ is stated in terms of the design variables $\boldsymbol{\rho}$ as follows:

$$\begin{aligned} \min_{\rho} \quad & C = \sum_i \boldsymbol{u}_{e,i}^T \boldsymbol{K}_{e,i} \boldsymbol{u}_{e,i} = \boldsymbol{f}^T \boldsymbol{u} && \forall i \in [0, \dots, N_e] \\ \text{s.t.} \quad & \frac{\sum_i \left(\bar{\tilde{\rho}}_i v_i\right) / V_0}{V^*} - 1 \leq 0 && \forall i \in [0, \dots, N_e] \qquad (\mathbb{T}_0) \\ & \boldsymbol{K}\boldsymbol{u} = \boldsymbol{f} \\ & 0 \leq \rho_i \leq 1. && \forall i \in [0, \dots, N_e] \end{aligned}$$

The design variables $\boldsymbol{\rho}$ are defined for every element of the structure as $\boldsymbol{\rho} = [\rho_1, \rho_2, \dots, \rho_{Ne}]^T$, with $\rho_i \in [0, 1]$, $\forall i \in [0, \dots, N_e]$. The physical densities $\bar{\tilde{\boldsymbol{\rho}}}$ are related to design variables through density filtering and threshold projection [13], as explained later in the document. V^* is the prescribed volume fraction that acts as constraint of the minimization problem, while v_i represents the area of the i-th element and V_0 the total area of the domain Ω. $\boldsymbol{K}\boldsymbol{u} = \boldsymbol{f}$ is the state equation of the problem and defines the elastic response of the structure to an external nodal load $\boldsymbol{f} = [f_1, f_2, \dots, f_{2M}]^T$. The global stiffness matrix $\boldsymbol{K}$ is assembled from the element stiffness matrix $\boldsymbol{K} = \sum_{i \in \Omega} \boldsymbol{K}_{e,i}$ and $\boldsymbol{K}_{e,i} = E_i \boldsymbol{K}_{e,0}$ where $\boldsymbol{K}_{e,0}$ represents the element stiffness matrix relative to the chosen type of element (linear or quadratic) and $E_i(\bar{\tilde{\rho}}_i)$ the Young's modulus of the i-th element.

13. Wang et al. (2011), 'On projection methods, convergence and robust formulations in topology optimization'

The material scheme used to interpolate between void and full material is the well known Solid Isotropic Material with Penalization Method (SIMP) [7, 14] approach. It is governed by the equation:

$$E_i(\bar{\tilde{\rho}}_i) = E_{\min} + \bar{\tilde{\rho}}_i^{\,p} (E_0 - E_{\min}), \tag{1.1}$$

7. Bendsøe (1989), 'Optimal shape design as a material distribution problem'

14. Bendsøe et al. (1999), 'Material interpolation schemes in topology optimization'

where the parameter p penalizes the intermediate densities and pushes the result to a black and white result. E_0 is the Young's modulus of the dense material and $E_{\min}$ is a small value used to avoid the global stiffness matrix $\boldsymbol{K}$ from being singular when $\bar{\tilde{\rho}}_i = 0$.

In this study we set these parameters to $E_0 = 1$, and $E_{\min} = 10^{-9}$. The value of the penalization parameter p is selected as $p = 3$ because in that way the intermediate densities respect the Hashin-Shtrikman (HS) bounds [14, 15]. This describes the boundaries of attainable isotropic material characteristics when dealing with composites (materials with microscopic structures) using two specified, linearly elastic, isotropic materials (in our case the solid and the empty phases).

15. Hashin et al. (1963), 'A variational approach to the theory of the elastic behaviour of multiphase materials'

16. Díaz et al. (1995), 'Checkerboard patterns in layout optimization'

17. Sigmund (1994), 'Design of Material Structures using Topology Optimization'

18. Sigmund (1997), 'On the Design of Compliant Mechanisms Using Topology Optimization'

Spatial filtering and projection Multiple approaches have been developed to solve the problems linked to the mesh discretization, such as mesh dependence or the checkerboard problem [16]. Filtering the sensitivity information of the optimization problem proved to be an effective approach to guarantee independence from mesh resolution

[17, 18]. In the present research we decided instead to directly filter the density field $\boldsymbol{\rho}$ using the 2D convolution operator [19]. The weight function w (or kernel) of the convolution is defined as:

19. Sigmund (2007), 'Morphology-based black and white filters for topology optimization'

$$w(d_j) = R - d_j, \quad j \in \mathbb{N}_{i,R} \tag{1.2}$$

where $\mathbb{N}_{i,R}$ represent the set of elements lying within a circle of radius R centered on the i-th element and d_j is the distance of the j-th element to the center of the filter (see Fig. 1.2).

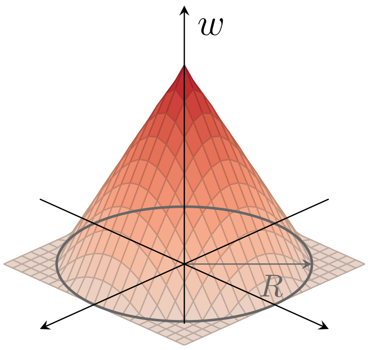

Figure 1.2: Kernel of the 2D convolution operator.

The filtered values of the design variable calculated as:

$$\tilde{\rho}_i = \frac{\sum_{j \in \mathbb{N}_{i,R}} w(d_j) v_j \rho_j}{\sum_{j \in \mathbb{N}_{i,R}} w(d_j) v_j}. \tag{1.3}$$

As the filtering phase produces a large quantity of gray elements, a smooth projection technique based on the *tanh* function is implemented [13]:

13. Wang et al. (2011), 'On projection methods, convergence and robust formulations in topology optimization'

$$\bar{\tilde{\rho}}_j = \frac{\tanh(\beta\eta) + \tanh(\beta(\tilde{\rho}_j - \eta))}{\tanh(\beta\eta) + \tanh(\beta(1 - \eta))}, \tag{1.4}$$

where β is a parameter that define the slope of this approximation function: the larger the value of β, the less intermediate elements are present in the structure topology. η is the threshold value of the projection. Using Equation 1.4 is not volume conservative for all values of η, and to stay conservative we use a volume-increasing filter [20]. The value of $\eta = 0.4$ is then chosen.

20. Ferrari et al. (2020), 'A new generation 99 line Matlab code for compliance topology optimization and its extension to 3D'

The derivative of the filtered density $\tilde{\boldsymbol{\rho}}$ with respect to the design variable $\boldsymbol{\rho}$ is written deriving Equation 1.3:

$$\frac{\partial \tilde{\rho}_i}{\partial \rho_j} = \frac{w(d_j) v_j}{\sum_{j \in \mathbb{N}_{i,R}} w(d_j) v_j}. \tag{1.5}$$

The sensitivity of the physical densities $\bar{\tilde{\boldsymbol{\rho}}}$ with respect to the filtered $\tilde{\boldsymbol{\rho}}$ can be written as:

$$\frac{\partial \bar{\tilde{\rho}}_j}{\partial \tilde{\rho}_j} = \beta \frac{1 - \tanh^2(\beta(\tilde{\rho}_j - \eta))}{\tanh(\beta\eta) + \tanh(\beta(1 - \eta))}. \tag{1.6}$$

Using the chain rule it is possible to write:

$$\frac{\partial h}{\partial \rho_i} = \sum_{j \in \mathbb{N}_{i,R}} \frac{\partial f}{\partial \bar{\tilde{\rho}}_j} \frac{\partial \bar{\tilde{\rho}}_j}{\partial \tilde{\rho}_j} \frac{\partial \tilde{\rho}_j}{\partial \rho_i}, \tag{1.7}$$

where h represents a generic function.

Objective and constraint funtions Up until this point, we have been focused on the compliance minimization formulation $\mathbb{T}_0$. Moving forward, we introduce the necessary modifications to transition into the volume minimization formulation with stress constraints. This formulation will be used to compare the continuous mesh with truss-link structure optimization.

The objective of the optimization is to minimize the volume of a structure subject to a specified load case. The volume of the structure V is expressed in percentage with respect to the total volume V_0 of the domain Ω:

$$V = \frac{1}{V_0} \sum_{i \in \Omega} \bar{\bar{\rho}}_i v_i, \tag{1.8}$$

where v_i is the elementary volume occupied by the i-th element. In this thesis, we assume that v_i is equal for all the elements, and thus Equation 1.8 is simplified as follows:

$$V = \frac{1}{N_e} \sum_{i \in \Omega} \bar{\bar{\rho}}_i, \tag{1.9}$$

The normalized local stress constraint g_{st} are formulated as:

$$\frac{\sigma_{VM,j}}{\sigma_L} - 1 \leq 0, \quad \forall j \in \Omega_{mat}(\boldsymbol{\rho}), \tag{g_{st}}$$

where $\Omega_{mat}(\boldsymbol{\rho}) \subseteq \Omega$ represents the design-dependent set of elements with a non-zero density, $\sigma_{VM,j}$ is the equivalent von Mises stress for the j-th element, and σ_L is the maximum allowable of the material.

A first difficulty that arises is that the stress constraints are defined only for the elements where $\bar{\bar{\rho}}_i > 0$, while $\bar{\bar{\rho}}_i \in [0, 1]$. Thus, the set of constraints changes during the optimization. This class of problems are called Mathematical Programs with Vanishing Constraints (MPVCs) [21] and are known for being difficult to solve with a gradient descent optimization algorithm. The original set of constraints g_{st} is then reformulated into an equivalent design-independent set of constraints $\bar{g}_{\text{st}}$ as follows [22]:

21. Achtziger et al. (2008), 'Mathematical programs with vanishing constraints'

22. Cheng et al. (1992), 'Study on Topology Optimization with Stress Constraints'

$$\bar{\bar{\rho}}_i \left(\frac{\sigma_{VM,i}}{\sigma_L} - 1 \right) \leq 0, \quad \forall i \in \Omega. \tag{$\bar{g}_{\text{st}}$}$$

Von Mises stress evaluation The evaluation of the equivalent stress of an element follows the formulation proposed by Von Mises. Let us take a four-nodes quadrilateral linear element with a single integration (or Gauss) point in the center and four $2a$ equal-length sides (see Fig. 1.3). If bilinear shape function are used to interpolate the displacement field, we can evaluate the deformations at the integration point as:

$$\begin{pmatrix}\varepsilon_x\\ \varepsilon_y\\ \gamma_{xy}\end{pmatrix} = \boldsymbol{B}_s\boldsymbol{q}_s, \text{ with } \boldsymbol{B}_s = \frac{1}{4a}\begin{pmatrix}-1 & 1 & 1 & -1 & 0 & 0 & 0 & 0\\ 0 & 0 & 0 & 0 & -1 & -1 & 1 & 1\\ -1 & -1 & 1 & 1 & -1 & 1 & 1 & -1\end{pmatrix}, \tag{1.10}$$

where $\boldsymbol{q}_s = (u_1, u_2, u_3, u_4, v_1, v_2, v_3, v_4)^T$ represents the vector of the displacement degrees of freedom of the element.

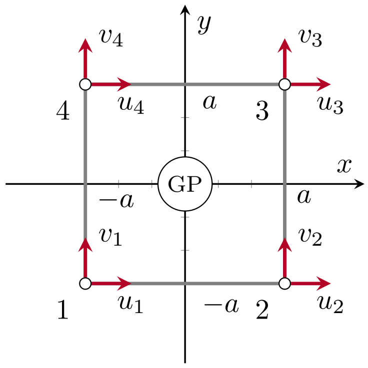

Figure 1.3: A four-node quadrilateral element. GP is the Gaussian integration point for which the equivalent stress is evaluated.

The stress tensor is evaluated using the elasticity Hooke's law in 2D as follows:

$$\begin{pmatrix}\sigma_x\\ \sigma_y\\ \tau_{xy}\end{pmatrix} = \boldsymbol{C}_e\begin{pmatrix}\varepsilon_x\\ \varepsilon_y\\ \gamma_{xy}\end{pmatrix}, \quad \text{with } \boldsymbol{C}_e = \frac{E}{1-\nu^2}\begin{pmatrix}1 & \nu & 0\\ \nu & 1 & 0\\ 0 & 0 & G\end{pmatrix}. \tag{1.11}$$

The equivalent Von Mises stress of the element can then be written as:

$$\langle\sigma_{VM}\rangle = \sqrt{\sigma_x^2 + \sigma_y^2 - \sigma_x\sigma_y + 3\tau_{xy}} \tag{1.12}$$

$$= \sqrt{\begin{pmatrix}\sigma_x & \sigma_y & \tau_{xy}\end{pmatrix}\begin{pmatrix}1 & -1/2 & 0\\ -1/2 & 1 & 0\\ 0 & 0 & 3\end{pmatrix}\begin{pmatrix}\sigma_x\\ \sigma_y\\ \tau_{xy}\end{pmatrix}} \tag{1.13}$$

$$= \sqrt{\boldsymbol{q}_s^T\boldsymbol{B}_s^T\boldsymbol{C}_e^T\boldsymbol{D}_{VM}\boldsymbol{C}_e\boldsymbol{B}_s\boldsymbol{q}_s}, \text{ with } \boldsymbol{D}_{VM} = \begin{pmatrix}1 & -1/2 & 0\\ -1/2 & 1 & 0\\ 0 & 0 & 3\end{pmatrix} \tag{1.14}$$

$$\langle\sigma_{VM}\rangle = \sqrt{\boldsymbol{q}_s^T\boldsymbol{S}\boldsymbol{q}_s}, \quad \text{with } \boldsymbol{S} = \boldsymbol{B}_s^T\boldsymbol{C}_e^T\boldsymbol{D}_{VM}\boldsymbol{C}_e\boldsymbol{B}_s \tag{1.15}$$

Microscopic and macroscopic stress In stress-constrained topology optimization the element stress is usually evaluated using the microscopic stress formulation, assuming that there is no direct correlation between stress and density [23]. Indeed, the use of the macroscopic stress in volume minimization optimization problems creates all-void design [24]. The properties that the microscopic stress should present are:

23. Duysinx et al. (1998), 'Topology optimization of continuum structures with local stress constraints'
24. Le et al. (2010), 'Stress-based topology optimization for continua'

(i) The stress criterion should be mathematically as simple as possible, as the relationship between Young's modulus and density. This permits a simple numerical implementation.
(ii) To mimic the real physical behavior, the microscopic stress should be inversely proportional to density.
(iii) The microscopic stress should converge to a non-zero value at zero density. This requisite is deduced from investigations into the asymptotic stress behavior in thin layers [25].

25. Verbart et al. (2017), 'A unified aggregation and relaxation approach for stress-constrained topology optimization'

The relation within stress and displacement is written as:

$$\langle \sigma_{VM} \rangle = \boldsymbol{C}_e(\langle E \rangle)\langle \boldsymbol{\varepsilon} \rangle \tag{1.16}$$

where the variables between angular brackets $\langle \ldots \rangle$ represent macroscopic variables.

Combining (i) and (ii) with Equations 1.1, and 1.16, the microscopic stress can be written as:

$$\boldsymbol{\sigma}_{VM} = \frac{\langle \sigma_{VM} \rangle}{\rho_e^q} = \rho_e^{p-q}\boldsymbol{C}_e(E_0)\langle \boldsymbol{\varepsilon} \rangle \tag{1.17}$$

where the exponent q is a number greater than 1.

One possible choice that satisfy all the requirements is $q = p$ [24–27]. Thus, the microscopic stress is defined as:

$$\boldsymbol{\sigma}_{VM} = \boldsymbol{C}_e(E_0)\langle \boldsymbol{\varepsilon} \rangle \tag{1.18}$$

From a physical perspective, the significance of microscopic stress becomes evident when considering an element with intermediate density and a porous microstructure. The microscopic stress presented in Equation 1.18 measures the stress of the microstructure. It is grounded in the assumption that the macroscopic deformations of the homogenized element generate within the microstructure of the element a stress state that remains unaffected by the density of the element itself.

24. Le et al. (2010), 'Stress-based topology optimization for continua'
25. Verbart et al. (2017), 'A unified aggregation and relaxation approach for stress-constrained topology optimization'
26. Holmberg et al. (2013), 'Stress constrained topology optimization'
27. Silva et al. (2019), 'Stress-constrained topology optimization considering uniform manufacturing uncertainties'

Constraints aggregation and relaxation When optimizing a structure with stress constraints using a NAND formulation, two primary challenges commonly arise:

(i) Is it known in the literature [28, 29] that stress-based topolgy optimization suffer from the *singular minima* (or *singularity*) problem: firstly observed on truss structure optimization [30], these *minima* are almost inaccessible to standard gradient-based optimizer, and they represent the *minima* of the optimization. This because achieving the optimal solution to a problem using continuous design variables may necessitate passing through a state where the optimization constraints are violated, i.e. the *minimum* is on a lower dimension compared to the design space. This problem is often solved using a technique called *constraints relaxation* [31].

(ii) The stress is a local measure, and thus a large set of constraints is generated when a reasonably fine mesh is used (one element, one constraint). This problem is often solved using a technique called *constraints aggregation* or *global constraints* [32].

Following the work developed by Verbart *et al.* [25], the lower bound

31. Cheng et al. (1997), 'ε-relaxed approach in structural topology optimization'
32. Silva et al. (2021), 'Local versus global stress constraint strategies in topology optimization'
25. Verbart et al. (2017), 'A unified aggregation and relaxation approach for stress-constrained topology optimization'

33. Kreisselmeier et al. (1979), 'Systematic Control Design by Optimizing a Vector Performance Index'

Kreisselmeier-Steinhauser (KS) function [33] is used to approximate the local relaxed stress constraint maximum. The authors discovered that employing lower-bound KS aggregation functions to approximate the maximum operator in stress-constrained topology optimization eliminates the need for stress constraint relaxation methods to address the singularity issue. This is because the lower-bound functions inherently offer a combined effect of constraints aggregation and relaxation. The KS aggregated stress constraint function is defined as follows:

$$G_{KS}^{L} = \frac{1}{P} \ln\left(\frac{1}{N_e} \sum e^{P\bar{g}_i}\right). \tag{1.19}$$

Its main advantage over other different formulations is that it uses a single hyperparameter P to control the aggregation and the relaxation of the constraints simultaneously.

Minimum volume formulation The NAND minimum volume formulation for continuous discretization is written Equations 1.9, and 1.19 as:

$$\begin{aligned} \min_{\rho} \quad & V = \frac{1}{N_e} \sum_{i\in\Omega} \bar{\bar{\rho}}_i, \\ \text{s.t.} \quad & G_{KS}^{L} = \frac{1}{P} \ln\left(\frac{1}{N_e} \sum_{i\in\Omega} e^{P\bar{g}_i}\right) \leq 0 \\ & \boldsymbol{Ku} = \boldsymbol{F} \\ & 0 \leq \rho_i \leq 1, \end{aligned} \tag{$\mathbb{T}_1$}$$

The optimization is carried out using a gradient descent optimization algorithm for which the sensitivities are given in analytical form. Using analytic gradients is in general more efficient than finite differences as it avoids the need for multiple function evaluations, making the optimization process faster and more precise.

Sensitivity analysis of the objective function The objective of this section is to quickly present the calculation of the analytical sensitivity of the volume with respect to the design variable ρ. Deriving Equation 1.9 we obtain:

$$\frac{\partial V}{\partial \bar{\bar{\rho}}_i} = \frac{1}{N_e}, \tag{1.20}$$

The sensitivity of the objective function can then be evaluated using Equations 1.20, 1.5, 1.6, and 1.7 as follows:

$$\frac{dV}{d\rho_i} = \sum_{j\in\mathbb{N}_{i,R}} \frac{\partial V}{\partial \bar{\bar{\rho}}_j} \frac{\partial \bar{\bar{\rho}}_j}{\partial \tilde{\rho}_j} \frac{\partial \tilde{\rho}_j}{\partial \rho_i}. \tag{1.21}$$

Sensitivity analysis of the constraint function This section focuses on the details of the calculation of how the constraint function G^L_{KS} changes with respect to the design variable $\boldsymbol{\rho}$.

As the constraint function $G^L_{KS} = G(\bar{\bar{\boldsymbol{\rho}}}, \boldsymbol{u}(\bar{\bar{\boldsymbol{\rho}}}))$ is explicitly and implicitly (via the relationship with $\boldsymbol{u}$) depending on $\bar{\bar{\boldsymbol{\rho}}}$, the first-order derivative is evaluated using the total derivative formula:

$$\frac{\partial G^L_{KS}}{\partial \bar{\bar{\rho}}_j} = \frac{dG}{d\bar{\bar{\rho}}_j} = \frac{\partial G}{\partial \bar{\bar{\rho}}_j} + \frac{\partial G}{\partial \boldsymbol{u}} \frac{d\boldsymbol{u}}{d\bar{\bar{\rho}}_j} \tag{1.22}$$

As function G^L_{KS} depends on $\boldsymbol{u}$ via the stresses σ_i, it is possible to write:

$$\frac{\partial G}{\partial \boldsymbol{u}} = \sum_{i \in \Omega} \left(\frac{\partial G}{\partial \sigma_i} \frac{\partial \sigma_i}{\partial \boldsymbol{u}} \right) \tag{1.23}$$

Combining Eq. 1.22 with Eq. 1.23, we obtain:

$$\frac{dG}{d\bar{\bar{\rho}}_j} = \underbrace{\frac{\partial G}{\partial \bar{\bar{\rho}}_j}}_{A} + \sum_{i \in \Omega} \left(\underbrace{\frac{\partial G}{\partial \sigma_i}}_{B} \underbrace{\frac{\partial \sigma_i}{\partial \boldsymbol{u}}}_{C} \right) \underbrace{\frac{d\boldsymbol{u}}{d\bar{\bar{\rho}}_j}}_{D} \tag{1.24}$$

We compute the four factors separately:

A - The first term represents the explicit relationship of G to the physical densities and its calculation is straightforward:

$$\frac{\partial G}{\partial \bar{\bar{\rho}}_j} = \frac{1}{P} \frac{\left(\frac{\sigma_{VM,j}}{\sigma_L} - 1 \right) \frac{1}{N_e} P e^{P \bar{g}_j}}{\frac{1}{N_e} \sum_k e^{P \bar{g}_k}} = \left(\frac{\sigma_{VM,j}}{\sigma_L} - 1 \right) \frac{e^{P \bar{g}_j}}{\sum_k e^{P \bar{g}_k}} \tag{1.25}$$

B - The second term can be calculated using the chain rule:

$$\frac{\partial G}{\partial \sigma_i} = \frac{\partial G}{\partial \bar{g}_i} \frac{\partial \bar{g}_i}{\partial \sigma_i} = \frac{1}{P} \frac{\frac{1}{N_e} P e^{P \bar{g}_i}}{\frac{1}{N_e} \sum_k e^{P \bar{g}_k}} \frac{\bar{\bar{\rho}}_i}{\sigma_L} = \frac{\bar{\bar{\rho}}_i}{\sigma_L} \frac{e^{P \bar{g}_i}}{\sum_k e^{P \bar{g}_k}} \tag{1.26}$$

C - We reformulate Eq. 1.15 to be written in global coordinates instead of local:

$$\sigma_i^2 = \boldsymbol{q}_s^T \boldsymbol{S} \boldsymbol{q}_s = \boldsymbol{u}^T |\boldsymbol{S_i}|_g \boldsymbol{u} \tag{1.27}$$

where $|\boldsymbol{S_i}|_g$ represents the matrix $\boldsymbol{S}$ of Equation 1.15written on global coordinates [2]. We can now differentiate Equation 1.27 with respect of the displacement field in global coordinates $\boldsymbol{u}$ to obtain:

$$\frac{\partial \sigma_i}{\partial \boldsymbol{u}} = \frac{|\boldsymbol{S_i}|_g \boldsymbol{u}}{\sigma_i} \tag{1.28}$$

2: The matrix $|\boldsymbol{S_i}|_g$ can be calculated using the very same assmebling approach used for the stiffness matrix $\boldsymbol{K}$ starting from the elemental stiffness matrix $\boldsymbol{K_e}$. As the global stiffness matrix $\boldsymbol{K}$, $|\boldsymbol{S_i}|_g$ is symmetric and sparse.

Equations 1.26, and 1.28 are now combined to obtain the result of the product of the **B** and **C** terms. As a result, the derivatives of G with respect to $\boldsymbol{u}$, are written as:

$$\frac{\partial G}{\partial \boldsymbol{u}} = \frac{\frac{\bar{\bar{\rho}}_j}{\sigma_L \sigma_j} e^{P\bar{g}_i}}{\sum_i e^{P\bar{g}_i}} |\boldsymbol{S}_j|_g \boldsymbol{u} \tag{1.29}$$

D - To calculate the last term, we take the static equilibrium equation $\boldsymbol{K}\boldsymbol{u} = \boldsymbol{f}$ and differentiating it with respect to the physical densities $\bar{\bar{\rho}}_j$, obtaining:

$$\frac{\partial \boldsymbol{K}}{\partial \bar{\bar{\rho}}_j}\boldsymbol{u} + \boldsymbol{K}\frac{\partial \boldsymbol{u}}{\partial \bar{\bar{\rho}}_j} = 0 \iff \frac{\partial \boldsymbol{u}}{\partial \bar{\bar{\rho}}_j} = -\boldsymbol{K}^{-1}\frac{\partial \boldsymbol{K}}{\partial \bar{\bar{\rho}}_j}\boldsymbol{u}, \tag{1.30}$$

where

$$\frac{\partial \boldsymbol{K}}{\partial \bar{\bar{\rho}}_j} = (E_0 - E_{\min})p\bar{\bar{\rho}}_j^{\,p-1}\boldsymbol{K}_{e,j}. \tag{1.31}$$

Equation 1.31 represent the well known first-derivative term of the global stiffness matrix $\boldsymbol{K}$ with respect of the physical densities $\bar{\bar{\rho}}_j$ when using SIMP material scheme [12]. We finally obtain the last term:

12. Bendsøe et al. (2004), *Topology Optimization*

$$\frac{d\boldsymbol{u}}{d\bar{\bar{\rho}}_j} = -\boldsymbol{K}^{-1}\left((E_0 - E_{\min})p\bar{\bar{\rho}}_j^{\,p-1}\boldsymbol{K}_e\right)\boldsymbol{u} \tag{1.32}$$

Combining Eq. 1.24, Eq. 1.25, Eq. 1.29, and Eq. 1.32, we finally obtain:

$$\frac{\partial G_{KS}^L}{\partial \bar{\bar{\rho}}_j} = \left(\frac{\sigma_{VM,j}}{\sigma_L} - 1\right)\frac{e^{P\bar{g}_j}}{\sum_k e^{P\bar{g}_k}} - \boldsymbol{K}^{-1}\frac{\partial G}{\partial \boldsymbol{u}}\left(\frac{\partial \boldsymbol{K}}{\partial \bar{\bar{\rho}}_j}\right)\boldsymbol{u} \tag{1.33}$$

To avoid the explicit calculation of $\boldsymbol{K}^{-1}$ we use the *adjoint method*[3]. Here is the linear system that, once solved, permits to calculate $\boldsymbol{\psi}$:

3: More information about the adjoint method used to analytically calculate the first-order derivatives can be found on the Martins *et al.* book [11].

$$\boldsymbol{K}\boldsymbol{\psi} = \frac{\partial G}{\partial \boldsymbol{u}} \iff \boldsymbol{\psi} = \boldsymbol{K}^{-1}\frac{\partial G}{\partial \boldsymbol{u}} \tag{1.34}$$

This formula is called *adjoint equation*. This equation is solved for $\boldsymbol{\psi}$ and the result used to evaluate:

$$\frac{\partial G_{KS}^L}{\partial \bar{\bar{\rho}}_j} = \left(\frac{\sigma_{VM,j}}{\sigma_L} - 1\right)\frac{e^{P\bar{g}_j}}{\sum_k e^{P\bar{g}_k}} - \boldsymbol{\psi}\left(\frac{\partial \boldsymbol{K}}{\partial \bar{\bar{\rho}}_j}\right)\boldsymbol{u} \tag{1.35}$$

where N represents the size of the square matrix describing the linear system. Eq. 1.35 represents the first-order derivative equation used to evaluate the sensitivity of the constraint function G_{KS}^L with respect to the physical densities $\bar{\bar{\boldsymbol{\rho}}}$. The value of $\boldsymbol{\psi}$ is calculated every iteration solving the linear system 1.34.

Solving linear system 1.34 instead of directly calculating the inverse matrix of $\boldsymbol{K}$ is more efficient from a performance perspective. The cost of solving a system using the Cholesky decomposition is $\mathcal{O}(N^3/3)$, while a matrix inversion is $\mathcal{O}(N^3)$.

The sensitivity of the aggregated contraint function with respect to the design variable $\boldsymbol{\rho}$ is evaluated using Equations 1.20, 1.5, 1.6, and 1.7 as follows:

$$\frac{dG^L_{KS}}{d\rho_i} = \sum_{j \in \mathbb{N}_{i,R}} \frac{\partial G^L_{KS}}{\partial \overline{\overline{\rho}}_j} \frac{\partial \overline{\overline{\rho}}_j}{\partial \widetilde{\rho}_j} \frac{\partial \widetilde{\rho}_j}{\partial \rho_i}. \tag{1.36}$$

1.1.2 Truss discretization SAND minimum volume formulation

We are now shifting our focus from continuous structures to discrete truss systems, describing the Truss Topology Optimization (TTO) (also knows in early literature as layout optimization), a structure optimization method that focuses on discrete structures. In his most used formulation, TTO aims at reducing material usage while meeting stress criteria using a SAND approach. The problem is already well-posed for the comparison with continuous discretization, and our intention is to now explore specific key concepts within its established framework.

Classical Michell structures The characteristics of these structures are described by some simple criteria that date to the end of the 19th and the beginning of the 20th century. When a structure is statically determinate — i.e. the structure is not a mechanism, and it is not over-constrained by the supports — the Maxwell theorem [34] states that:

34. Maxwell (1870), 'I.—On Reciprocal Figures, Frames, and Diagrams of Forces'

$$\sum_{\forall i | q_i > 0} \ell_i q_i + \sum_{\forall i | q_i < 0} \ell_i q_i = \text{const.} \tag{1.37}$$

where ℓ_i and q_i represent the length and the axial force of the i-th member, respectively. The constant value at the right of Equation 1.37 depends on the nature of the boundary conditions and the material used. The Maxwell theorem dictates that any increment in compression forces must be counterbalanced by an equivalent increase in tension forces when the structure remains topologically unchanged. So for statically determinate structures the structure layout is not influenced by the ratio between σ_c and σ_t, the Young's modulus E of the material, nor the force magnitude.

Starting from Maxwell's findings, Michell theorized two further criteria for optimal truss structures [35] valid when the maximum allowable stress is equal in tension and compression ($\sigma_t = \sigma_c$) and when the supports of the structure are statically determinate. The first one states that all the members of an optimal structure should present internal stress equal in magnitude to the maximum allowable value of the material - i.e. the structure is *fully stressed*. The second criterion asserts that the strain of all the members of the structure should be equal and there should be no other point having a strain higher than this value. As formulated, these two criteria are known as the Michell criteria. The second criterion was later generalized by Hemp [4] as:

35. Michell (1904), 'The limits of economy of material in frame-structures'

4. Hemp (1973), *Optimum Structures*

$$-\frac{1}{\sigma_C} \leq \varepsilon \leq \frac{1}{\sigma_T} \tag{1.38}$$

Compared to the second Michell criterion, Equation 1.38 permits to correctly identify the minimum volume structure even when different strength values for compression and tension and different support types are taken. These criteria are known as the Michell-Hemp criteria.

Plastic material formulation The rigid-plastic formulation characterizes the material as entirely rigid up to the point of reaching the yield stress, denoted as σ_y, and subsequently assumes a constant stress level of σ_y once that threshold is exceeded. This formulation is a clear consequence of the application of the Michell-Hemp criteria and has thus been used in the very first work of layout optimization (also known as TTO) [2–4].

2. Dorn et al. (1964), 'Automatic design of optimal structures'
3. Chan (1964), 'Optimum structural design and linear programming'
4. Hemp (1973), *Optimum Structures*

The ground structure approach The ground structure is a framework composed of various structural members that connect specified points or nodes in two- or three-dimensional space (see Fig. 1.4). These members can take the form of beams, columns, wires, or bars elements, depending on the specific structural requirements. In this thesis we will deal with trusses, and so the chosen element is the bar. Since the nodes within the ground structure are considered pin-joints, all straight members exclusively face either tension or compression loads.

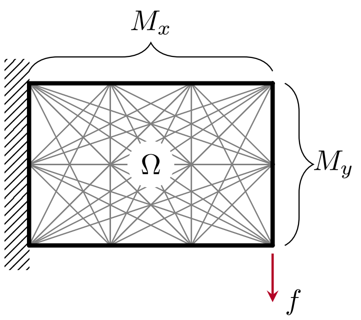

Figure 1.4: The domain Ω is discretized using a set of straight members connecting a set of nodes. THis framework is known as ground structure.

Depending on how the connectivity of the grid of nodes is, we can experience very different ground structures. In a fully connected ground structure, every node within the system is linked to every other node, resulting in a dense and redundant structural configuration. The number of bars N_{el} of a fully connected ground structure can be determined using the following formula:

$$N_{\mathrm{el}} = \frac{M \cdot (M-1)}{2} \tag{1.39}$$

where M represent the number of nodes of the structure.

In classic works, the ground structure is used as the start of the optimization, where the optimized structure is obtained as a subset of the initial ground structure, but multiple alternative approaches have been proposed since then, e.g. starting from a very coarse ground structure that is enriched during the analysis [36], or giving the nodes of a coarse ground structure the possibility to move, during [37–39], or after the optimization, simultaneously reducing the number of active members of the solution [40, 41].

36. Gilbert et al. (2003), 'Layout optimization of large-scale pin-jointed frames'
37. Pedersen (1973), 'Optimal Joint Positions for Space Trusses'
38. Achtziger (2007), 'On simultaneous optimization of truss geometry and topology'
39. Descamps et al. (2013), 'A lower-bound formulation for the geometry and topology optimization of truss structures under multiple loading'
40. He et al. (2015), 'Rationalization of trusses generated via layout optimization'
41. Lu et al. (2023), 'Reducing the number of different members in truss layout optimization'

Optimization formulation The volume minimization formulation with maximum stress constraints is stated in terms of members' cross-sectional areas $\boldsymbol{a}$ and member forces $\boldsymbol{q}$ as follows:

$$\begin{aligned} \min_{\boldsymbol{a},\boldsymbol{q}} \quad & V = \boldsymbol{\ell}^T \boldsymbol{a} && \text{(Volume)} \\ \text{s.t.} \quad & \boldsymbol{B}_s \boldsymbol{q} = \boldsymbol{f} && \text{(Force equilibrium)} \\ & -\sigma_c \boldsymbol{a} \leq \boldsymbol{q} \leq \sigma_t \boldsymbol{a} && \text{(Stress constraints)} \\ & \boldsymbol{a} \geq 0, \end{aligned} \qquad (\mathbb{P}_0)$$

where $\boldsymbol{B}_s$ is a $N_{\text{dof}} \times N_{\text{el}}$ matrix containing the direction cosines of the j-th member with respect to the i-th degree of freedom to calculate the nodal force equilibrium, and where N_{dof} is the number of Degrees Of Freedom (DOFs), equal to $2M$ or $3M$ for a two- or a three-dimensional load case, respectively. $\boldsymbol{q} = [q_1, q_2, \ldots, q_{N_{\text{el}}}]^T$ is the vector containing the internal member forces, with a positive sign when in tension, caused by the external load $\boldsymbol{f} = [f_1, f_2, \ldots, f_{N_{\text{dof}}}]^T$. The state variable $\boldsymbol{a} = [a_1, a_2, \ldots, a_{N_{\text{el}}}]^T$ represents the cross-sectional area of the N_{el} members of the structure. σ_c and σ_t are the compressive and tensile maximum allowable stresses of the material, respectively. This formulation takes into account only the linear behaviur of the structure and is equivalent to the original and well-studied member force formulation [2, 12]. add joint cost

2. Dorn et al. (1964), 'Automatic design of optimal structures'
12. Bendsøe et al. (2004), *Topology Optimization*

1.2 Comparison between continuous and truss discretization

In the upcoming discussion, we will be comparing the optimized structures using discrete and continuous meshes. Our primary objective in this comparison is to gain a comprehensive understanding of the application limits inherent in these two structural discretization methods. If, indeed, we identify such limitations, the aim is to discern and define them.

Since our interest in ultralight structures, we are especially interested in comparing the results of both optimization methods when dealing with a common load case at different volumes. Since we can't directly control volume in our formulation, we will adjust material properties to influence the volume fraction of the optimized structure. For this comparative analysis, we have selected three key performance metrics: volume fraction V_f, structural compliance C, and the maximum material allowable σ_L. Among these, we classify stress limit as the active metric used to influence the optimization, while volume and compliance are the objective of the optimization and a passive metric, respectively. In addition to the aforementioned performance metrics, we will also track the execution time of the algorithms.

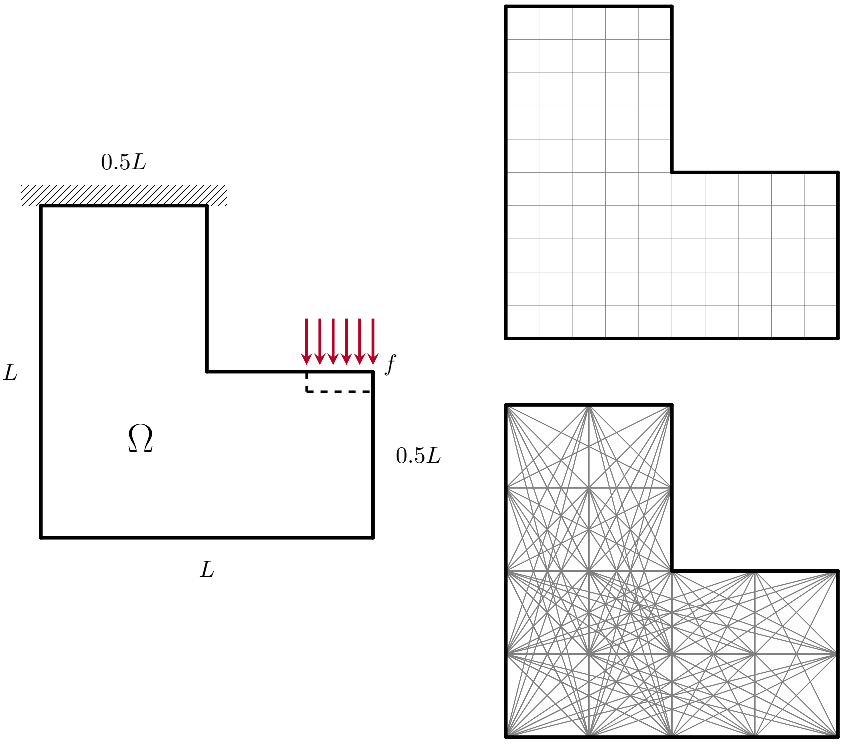

Figure 1.5: testtesttest

1.2.1 Definition of a common test case

the L shape is one of the most used load case benchmark for stress based topology optimization find citations

descrizione del load case

fai margin table con i dati materiale

1.2.2 Numerical application

fai margin table con i dati usati per la risoluzione degli argoritmi definition of the figure of merits that are used to control the volume and the one that are compared: stress, volume, compliance (passive). additionally we will monitor the computational time as well

start with TO add image with 4 different solutions 4 different stress

Now TTOfai rerun per nuova colormap interesting how the solution is not influenced by the number of nodes. expecially at low volume fration vs TO that needs more an more elements the finer we want to go speaks about the fact that the solution doesn't change the topology. why that? Hemp michell criteria as already explained add image

$$PL/\sigma \tag{1.40}$$

[42]

42. Lewiński et al. (1994), 'Extended exact solutions for least-weight truss layouts—Part I'

Table 1.1: TTO

σ_L	V_f	C	**Min** λ	**Time [s]**
50.0	0.12	23 282	111.7	66
20.0	0.31	9313	70.6	69
10.0	0.62	4656	49.9	78
8.0	0.78	3725	44.7	75
6.0	1.03	2794	38.7	70
5.0	1.24	2328	35.3	84
4.0	1.55	1863	31.6	78
3.0	2.07	1397	27.4	85
2.0	3.10	931	22.3	85
1.0	6.21	466	15.8	77
0.9	6.90	419	15.0	80
0.8	7.76	373	14.1	81
0.7	8.87	326	13.2	76
0.6	10.35	279	12.2	80
0.5	12.42	233	11.2	82

1.2.3 Discussion

segna da qualche parte la slenderness maximum minimum slenderness ratio λ (ratio between the length and the radius of gyration of the bar) of a bar is

Compliance-volume graph

Compliance-stress graph

Stress-volume graph time comparison

parla del fatto che lo stress calcolato dalla TO ha un overshoot dovuto alla gksl

"The methods allow for a determination of the topology of a mechanical element and give useful information on the form of the boundaries of the optimal shape. For moderately low volume fractions the lay-out of truss-like structures is predicted, but for very low volume fractions it is recommended that the traditional lay-out theory be employed, as described by Rozvany (1984)." [7]

"Also, for moderately low volume fractions the method works like a method for lay-out of truss-like structure" [6]

but the performance gap has never been mesurated nor the domain of appicability. here's wy of this chapter. on the top of that these assumptions where on complaince formulations

7. Bendsøe (1989), 'Optimal shape design as a material distribution problem'

6. Bendsøe et al. (1988), 'Generating optimal topologies in structural design using a homogenization method'

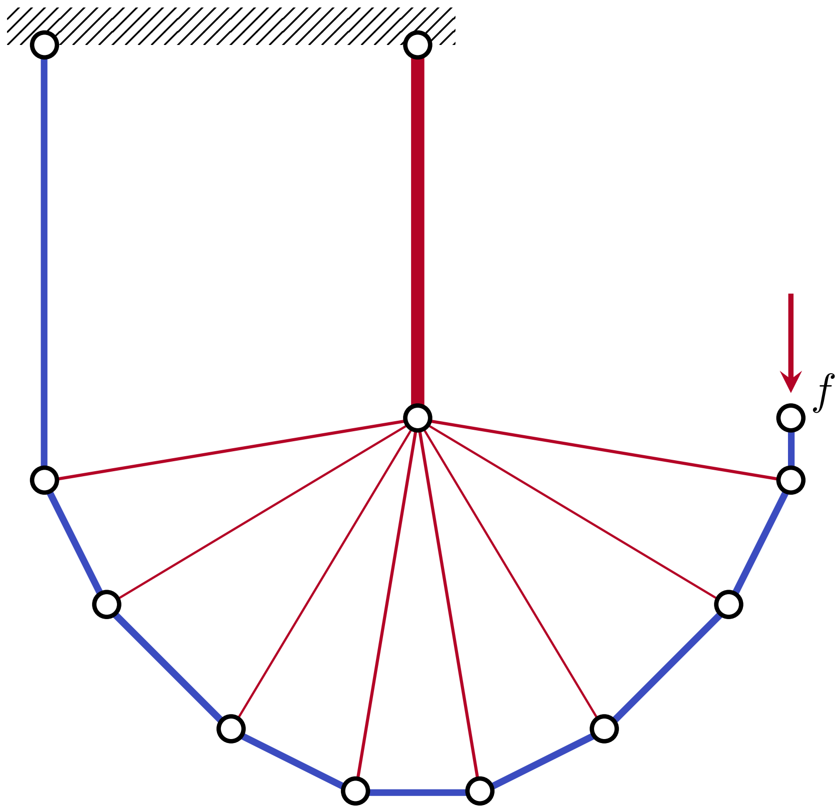

Figure 1.6: testtesttest

One should consider that SAND approaches usually increases the number of design variables considerably. Nevertheless, in truss topology problems this is less concerning, as the ground structure approach results in numerous cross-sectional area design variables and fewer displacement-related ones. This, however, does not hold true when dealing with a continuous mesh, where the NAND approach reduces considerably the number of design variables.

When stress no self adjoint SAND could be benificial however to add more constraints such as stress buckling and displacements because in that way no self adjoint

calculation time

problems of the tto (open to the new chapter)

1.3 Conclusion

we have introduced the formulation we have run the analysis on a common load case we have compared the results we have selected the truss topology optimization BUT Open to the new chapter

Bibliography

[1] Stragiotti, Enrico et al., 'Towards manufactured lattice structures: a comparison between layout and topology optimization', *AeroBest 2021 International Conference on Multidisciplinary Design Optimization of Aerospace Systems. Book of proceedings*, Lisbon, Portugal: ECCOMAS, July 2021, pp. 229–244. cited on page 1

[2] Dorn, W. S., Gomory, Ralph E., and Greenberg, H., 'Automatic design of optimal structures', *J. Mécanique* (1964). cited on pages 1, 12, 13

[3] Chan, H. S. Y., 'Optimum structural design and linear programming', *College of Aeronautics Report Aero 175* (1964), Publisher: College of Aeronautics Cranfield. cited on pages 1, 12

[4] Hemp, W. S., *Optimum Structures*. Clarendon Press, 1973, Google-Books-ID: cJhpAAAAMAAJ. cited on pages 1, 11, 12

[5] Sankaranarayanan, S., Haftka, Raphael T., and Kapania, Rakesh K., 'Truss topology optimization with simultaneous analysis and design', *AIAA Journal* 32.2 (Feb. 1994), pp. 420–424.
DOI: 10.2514/3.12000 cited on page 1

[6] Bendsøe, Martin Philip and Kikuchi, Noboru, 'Generating optimal topologies in structural design using a homogenization method', *Computer Methods in Applied Mechanics and Engineering* 71.2 (Nov. 1988), pp. 197–224.
DOI: 10.1016/0045-7825(88)90086-2 cited on pages 1, 15

[7] Bendsøe, M. P., 'Optimal shape design as a material distribution problem', *Structural optimization* 1.4 (Dec. 1989), pp. 193–202.
DOI: 10.1007/BF01650949 cited on pages 1, 3, 15

[8] Sigmund, Ole, 'Materials with prescribed constitutive parameters: An inverse homogenization problem', *International Journal of Solids and Structures* 31.17 (Sept. 1994), pp. 2313–2329.
DOI: 10.1016/0020-7683(94)90154-6 cited on page 1

[9] Zhang, Weihong and Sun, Shiping, 'Scale-related topology optimization of cellular materials and structures', *International Journal for Numerical Methods in Engineering* 68.9 (2006), _eprint: https://onlinelibrary.wiley.com/doi/pdf/10.1002/nme.1743, pp. 993–1011.
DOI: 10.1002/nme.1743 cited on page 1

[10] Tortorelli, D. A. and Michaleris, P., 'Design sensitivity analysis: Overview and review', *Inverse Problems in Engineering* 1.1 (Oct. 1994), Publisher: Taylor & Francis _eprint: https://doi.org/10.1080/174159794088027573, pp. 71–105.
DOI: 10.1080/174159794088027573 cited on page 2

[11] Martins, J.R.R.A. and Ning, A., *Engineering Design Optimization*. Cambridge University Press, 2021. cited on pages 2, 10

cited on pages 2, 10, 13
[12] Bendsøe, Martin P. and Sigmund, Ole, *Topology Optimization*. Berlin, Heidelberg: Springer Berlin Heidelberg, 2004.

cited on pages 3, 4
[13] Wang, Fengwen, Lazarov, Boyan Stefanov, and Sigmund, Ole, 'On projection methods, convergence and robust formulations in topology optimization', *Structural and Multidisciplinary Optimization* 43.6 (June 2011), pp. 767–784.
DOI: 10.1007/s00158-010-0602-y

cited on page 3
[14] Bendsøe, M. P. and Sigmund, O., 'Material interpolation schemes in topology optimization', *Archive of Applied Mechanics* 69.9 (Nov. 1999), pp. 635–654.
DOI: 10.1007/s004190050248

cited on page 3
[15] Hashin, Z. and Shtrikman, S., 'A variational approach to the theory of the elastic behaviour of multiphase materials', *Journal of the Mechanics and Physics of Solids* 11.2 (Mar. 1963), pp. 127–140.
DOI: 10.1016/0022-5096(63)90060-7

cited on page 3
[16] Díaz, A. and Sigmund, O., 'Checkerboard patterns in layout optimization', *Structural optimization* 10.1 (Aug. 1995), pp. 40–45.
DOI: 10.1007/BF01743693

cited on pages 3, 4
[17] Sigmund, Ole, 'Design of Material Structures using Topology Optimization', PhD thesis, Technical University of Denmark, DK-2800 Lyngby, 1994.

cited on pages 3, 4
[18] Sigmund, Ole, 'On the Design of Compliant Mechanisms Using Topology Optimization', *Mechanics of Structures and Machines* 25.4 (Jan. 1997), pp. 493–524.
DOI: 10.1080/08905459708945415

cited on page 4
[19] Sigmund, Ole, 'Morphology-based black and white filters for topology optimization', *Structural and Multidisciplinary Optimization* 33.4 (Apr. 2007), pp. 401–424.
DOI: 10.1007/s00158-006-0087-x

cited on page 4
[20] Ferrari, Federico and Sigmund, Ole, 'A new generation 99 line Matlab code for compliance topology optimization and its extension to 3D', *Structural and Multidisciplinary Optimization* 62.4 (Oct. 2020), pp. 2211–2228.
DOI: 10.1007/s00158-020-02629-w

cited on page 5
[21] Achtziger, Wolfgang and Kanzow, Christian, 'Mathematical programs with vanishing constraints: optimality conditions and constraint qualifications', *Mathematical Programming* 114.1 (July 2008), pp. 69–99.
DOI: 10.1007/s10107-006-0083-3

cited on page 5
[22] Cheng, Gengdong and Jiang, Zheng, 'Study on Topology Optimization with Stress Constraints', *Engineering Optimization* 20.2 (Nov. 1992), pp. 129–148.
DOI: 10.1080/03052159208941276

[23] Duysinx, P. and Bendsøe, M. P., 'Topology optimization of continuum structures with local stress constraints', *International Journal for Numerical Methods in Engineering* 43.8 (1998), pp. 1453–1478.
DOI: 10.1002/(SICI)1097-0207(19981230)43:8<1453::AID-NME480>3.0.CO;2-2 cited on page 6

[24] Le, Chau et al., 'Stress-based topology optimization for continua', *Structural and Multidisciplinary Optimization* 41.4 (Apr. 2010), pp. 605–620.
DOI: 10.1007/s00158-009-0440-y cited on pages 6, 7

[25] Verbart, Alexander, Langelaar, Matthijs, and Keulen, Fred van, 'A unified aggregation and relaxation approach for stress-constrained topology optimization', *Structural and Multidisciplinary Optimization* 55.2 (Feb. 2017), pp. 663–679.
DOI: 10.1007/s00158-016-1524-0 cited on pages 6, 7

[26] Holmberg, Erik, Torstenfelt, Bo, and Klarbring, Anders, 'Stress constrained topology optimization', *Structural and Multidisciplinary Optimization* 48.1 (2013), pp. 33–47.
DOI: 10.1007/s00158-012-0880-7 cited on page 7

[27] Silva, Gustavo Assis da, Beck, André Teófilo, and Sigmund, Ole, 'Stress-constrained topology optimization considering uniform manufacturing uncertainties', *Computer Methods in Applied Mechanics and Engineering* 344 (Feb. 2019), pp. 512–537.
DOI: 10.1016/j.cma.2018.10.020 cited on page 7

[28] Rozvany, G.I.N., 'On design-dependent constraints and singular topologies', *Structural and Multidisciplinary Optimization* 21.2 (Apr. 2001), pp. 164–172.
DOI: 10.1007/s001580050181 cited on page 7

[29] Stolpe, Mathias, 'On Models and Methods for Global Optimization of Structural Topology', Publisher: Matematik, PhD thesis, 2003. cited on page 7

[30] Sved, G. and Ginos, Z., 'Structural optimization under multiple loading', *International Journal of Mechanical Sciences* 10.10 (Oct. 1968), pp. 803–805.
DOI: 10.1016/0020-7403(68)90021-0 cited on page 7

[31] Cheng, G. D. and Guo, X., 'ε-relaxed approach in structural topology optimization', *Structural optimization* 13.4 (June 1997), pp. 258–266.
DOI: 10.1007/BF01197454 cited on page 7

[32] Silva, Gustavo Assis da et al., 'Local versus global stress constraint strategies in topology optimization: A comparative study', *International Journal for Numerical Methods in Engineering* 122.21 (2021), _eprint: https://onlinelibrary.wiley.com/doi/pdf/10.1002/nme.6781, pp. 6003–6036.
DOI: 10.1002/nme.6781 cited on page 7

cited on page 8

[33] Kreisselmeier, G. and Steinhauser, R., 'Systematic Control Design by Optimizing a Vector Performance Index', *IFAC Proceedings Volumes*, IFAC Symposium on computer Aided Design of Control Systems, Zurich, Switzerland, 29-31 August 12.7 (Sept. 1979), pp. 113–117.
DOI: 10.1016/S1474-6670(17)65584-8

cited on page 11

[34] Maxwell, J. Clerk, 'I.—On Reciprocal Figures, Frames, and Diagrams of Forces', *Earth and Environmental Science Transactions of The Royal Society of Edinburgh* 26.1 (1870), Publisher: Royal Society of Edinburgh Scotland Foundation, pp. 1–40.
DOI: 10.1017/S0080456800026351

cited on page 11

[35] Michell, A. G. M., 'The limits of economy of material in frame-structures', *The London, Edinburgh, and Dublin Philosophical Magazine and Journal of Science* 8.47 (Nov. 1904), Publisher: Taylor & Francis _eprint: https://doi.org/10.1080/14786440409463229, pp. 589–597.
DOI: 10.1080/14786440409463229

cited on page 12

[36] Gilbert, Matthew and Tyas, Andrew, 'Layout optimization of large-scale pin-jointed frames', *Engineering Computations* 20.8 (Dec. 2003), pp. 1044–1064.
DOI: 10.1108/02644400310503017

cited on page 12

[37] Pedersen, Pauli, 'Optimal Joint Positions for Space Trusses', *Journal of the Structural Division* 99.12 (Dec. 1973), Publisher: American Society of Civil Engineers, pp. 2459–2476.
DOI: 10.1061/JSDEAG.0003669

cited on page 12

[38] Achtziger, Wolfgang, 'On simultaneous optimization of truss geometry and topology', *Structural and Multidisciplinary Optimization* 33.4 (Apr. 2007), pp. 285–304.
DOI: 10.1007/s00158-006-0092-0

cited on page 12

[39] Descamps, Benoît and Filomeno Coelho, Rajan, 'A lower-bound formulation for the geometry and topology optimization of truss structures under multiple loading', *Structural and Multidisciplinary Optimization* 48.1 (July 2013), pp. 49–58.
DOI: 10.1007/s00158-012-0876-3

cited on page 12

[40] He, L. and Gilbert, M., 'Rationalization of trusses generated via layout optimization', *Structural and Multidisciplinary Optimization* 52.4 (Oct. 2015), pp. 677–694.
DOI: 10.1007/s00158-015-1260-x

cited on page 12

[41] Lu, Hongjia and Xie, Yi Min, 'Reducing the number of different members in truss layout optimization', *Structural and Multidisciplinary Optimization* 66.3 (Feb. 2023), p. 52.
DOI: 10.1007/s00158-023-03514-y

[42] Lewiński, T., Zhou, M., and Rozvany, G. I. N., 'Extended exact solutions for least-weight truss layouts—Part I: Cantilever with a horizontal axis of symmetry', *International Journal of Mechanical Sciences* 36.5 (1994), pp. 375–398.
DOI: 10.1016/0020-7403(94)90043-4 cited on page 14